tvst

Article

Quantitative Handheld Swept-Source Optical Coherence Tomography Angiography in Awake Preterm and Full-Term Infants

Kanheng Zhou[1,2], Shaozhen Song[2], Alex Legocki[3], Yuxuan Cheng[2], Leona Ding[3], Kasra A. Rezaei[3], Ruikang K. Wang[2,3], and Michelle T. Cabrera[3,4]

[1] School of Science and Engineering, University of Dundee, Dundee, UK
[2] Department of Bioengineering, University of Washington, Seattle, WA, USA
[3] Department of Ophthalmology, University of Washington, Seattle, WA, USA
[4] Division of Ophthalmology, Seattle Children's Hospital, Seattle, WA, USA

Correspondence: Michelle T. Cabrera, OA.9.220 Ophthalmology, 4800 Sand Point Way NE, Seattle, WA 98105, USA.
e-mail: cabreram@uw.edu

Received: July 20, 2020
Accepted: October 20, 2020
Published: December 14, 2020

Keywords: optical coherence tomography angiography; retinopathy of prematurity; infants

Citation: Zhou K, Song S, Legocki A, Cheng Y, Ding L, Rezaei KA, Wang RK, Cabrera MT. Quantitative handheld swept-source optical coherence tomography angiography in awake preterm and full-term infants. Trans Vis Sci Tech. 2020;9(13):19, https://doi.org/10.1167/tvst.9.13.19

Purpose: To compare retinal vascular parameters acquired by handheld swept-source optical coherence tomography angiography (SS-OCTA) between nonsedated preterm and full-term infants.

Methods: Preterm and full-term infants at the University of Washington Medical Center were enrolled. Retinal angiograms (nominal size ~7 × 7 mm^2) were obtained at each routine retinopathy of prematurity (ROP) screening session for preterms and once during the first 72 hours of life for full-terms. Macular vessel area density and nonperfusion area were evaluated on the binarized vasculature map in both small (1.5 × 1.5 mm) and large (3 × 3 mm) quadrants. Average vessel diameter and tortuosity values were obtained from each large vessel branch (length >200 µm). All vascular analyses used previously published algorithms.

Results: Handheld SS-OCTA captured 31 of 55 (56%) high-quality volumes on 8 awake preterm infants (gestational age 28 ± 4 weeks, birth weight 891 ± 314 g, postmenstrual age at first imaging session 37 ± 2 weeks) and 48 of 54 (89%) volumes on 12 awake full-term infants (gestational age 39 ± 1 weeks, birth weight 3405 ± 329 g). Signal-to-noise ratio was 5.08 ± 1.52 dB in preterm and 4.90 ± 1.12 dB in full-term infants. Preterm infants had higher mean large vessel tortuosity compared to full-term infants ($P = 0.004$). The large nasal quadrant vessel area density of infants with stage 3 and/or pre-plus or worse ROP was higher than other preterm infants ($P = 0.007$).

Conclusions: Although inadequate image quality limited usable imaging sessions, handheld SS-OCTA achieved adequate signal-to-noise ratio in nonsedated infants for quantitative retinal vascular parameter analysis.

Translational Relevance: Large- and small-vessel parameters were associated with prematurity and ROP severity, respectively.

Introduction

Retinopathy of prematurity (ROP) is a vasoproliferative disorder occurring in premature infants whereby immature retinal vasculature is introduced to a relatively hyperoxic environment, leading to neovascularization and, occasionally, retinal detachment.[1,2] ROP remains the leading cause of childhood preventable blindness in both the developing and developed world, despite advances in treatment.[3–5]

Handheld optical coherence tomography (OCT) is a noncontact and noninvasive imaging technique for detailed assessment of retinal microanatomy in supine infants.[6,7] Subclinical morphologic findings in the retina and vitreous, such as punctate hyperreflective vitreous opacities, vitreous bands, preretinal tissue, epiretinal membrane, cystoid macular edema,

retinoschisis, retinal detachment, and cross-sectional retinal vascular changes associated with plus disease, have been visualized using handheld OCT at the time of ROP screening.[8–13]

To visualize the retinal vasculature, indirect ophthalmoscopy, retinal fundus photography, and fluorescein angiography are traditionally employed. However, these methods are variably limited by lack of microvascular detail, lack of objective measurements, and necessity for venous injection of fluorescein dye.[14–17] More recently, increased acquisition speed has allowed for performing swept-source OCT angiography (SS-OCTA) on infants.[18–26] Our group reported a portable handheld clinical prototype SS-OCTA system optimized for imaging awake infants.[22] The handheld OCTA probe features a unique on-probe display for directly previewing the OCT B-scan results, a built-in iris viewer for rapidly aligning the probe with the patient's optical axis, and joystick controls to adjust the reference optical delay and fiber polarization state. The capability of this system was demonstrated on healthy adults and nonsedated preterm and full-term infants with high-quality four-layer OCTA (superficial retina, deep retina, choriocapillaris, and deep choroid).[22,27]

The clinical relevance of quantitative retinal vascular morphologic parameters assessed from OCTA images has been well established in the adult retinal literature.[28] For example, vessel area density, blood perfusion, and vessel diameter quantified from OCTA were identified as markers for diabetic retinopathy[29–32] and glaucoma.[33–40] Vessel tortuosity assessed from OCTA demonstrated diagnostic potential in diabetic retinopathy,[41,42] familial retinal arteriolar tortuosity,[43] and branch retinal vein occlusion.[44] In contrast, less literature has been published on quantitative OCTA imaging in the infant population. Hsu et al.[24] used an investigational Spectralis with Flex module device (Heidelberg Engineering, Heidelberg, Germany) to quantify foveal avascular zone (FAZ), vessel area density, and vessel length density in sedated infants. Compared to older children, their work identified retinal vascular variation across age, race, and axial length. Kothari et al.[26] identified small FAZs among seven extreme low birth weight infants with ROP. Beyond measuring the FAZ, quantitative OCTA retinal microvasculature and large blood vessel parameters in preterm infants with ROP have not been reported so far. An understanding of retinal vascular features using OCT in prematurity may provide new opportunities to detect ROP-related vascular pathologies.

In this study, we compared quantitative retinal microvasculature and large retinal blood vessel parameters among preterm infants screened for ROP and full-term normal newborn controls using our novel handheld clinical prototype SS-OCTA system with the goal to demonstrate feasibility of this imaging approach in awake infants.

Methods

Participants

Eight premature infants (16 eyes) and 12 full-term infants (24 eyes) were enrolled in this study. Among premature infants, five infants included in the previous studies[22,27] were also included in this study. The study was approved by the institutional review board of Seattle Children's Hospital and the University of Washington (Seattle, Washington), which also conformed to the tenets of the Declaration of Helsinki and the Health Insurance Portability and Accountability Act. Informed consent was obtained from the legal guardians of each neonate prior to imaging after explaining the nature and possible consequences of the study.

Consecutive preterm infants in the University of Washington Medical Center neonatal intensive care unit undergoing routine clinical ROP examinations were eligible for the study. Criteria for ROP screening were defined as less than 30 weeks' gestation, less than a 1500-g birth weight, or with an unstable clinical course based on neonatologist discretion. Consecutive full-term newborn infants in the University of Washington Maternal Infant Center were also eligible for the study if they had a gestational age greater than 37 weeks and were at least 12 hours old at the time of imaging. In order to minimize logistical burden for the unit, full-term infants whose family had significant social challenges (e.g., drug addiction, Child Protective Services involvement, controversial guardianship, or major behavioral problems) were not approached for this study.

Handheld SS-OCTA System

An investigational prototype handheld SS-OCTA system developed at the University of Washington, Seattle, in the laboratory of Ruikang Wang, PhD, was used for all imaging sessions, described in detail previously.[22] Briefly, the system utilized a 200-kHz A-scan rate swept-source laser with a central wavelength of 1051 nm and a spectral tuning range of 105.2 nm, providing a measured axial resolution of ~6 μm in tissue. The lateral resolution on the retina was calculated to be ~16 μm (for a typical 6.3 × 6.3-mm field of view in infants sampled at 400 × 400 A-scans).

The optical power emitted from the handheld probe was approximately 1.9 mW at the cornea and within the safety limits established by the American National Standards Institute.[45] The largest field of view that this handheld SS-OCTA system could provide was about 40 degrees.

Imaging Protocol

Preterm infants were imaged on the same day as each routine ROP examination, and full-term infants were imaged only once during the first 72 hours of life prior to discharge. Imaging procedures were previously described.[22] Briefly, all infants were placed in the supine position, and the iris viewer was used to center the probe over the pupil. The reference delay and polarization were adjusted on the probe to center and maximize the intensity of the B-scan on the display. Finally, refractive error was accounted for (if necessary) by manually adjusting the probe's lens before starting data acquisition. Each imaging session was restricted to a total of 15 minutes for both eyes. Pupils were dilated by applying an ophthalmic solution containing phenylephrine hydrochloride, 1%, and cyclopentolate, 0.2% (Cyclomydril; Alcon Laboratories, Fort Worth, TX, USA), twice, 5 minutes apart, at least 40 minutes before all imaging sessions. No eyelid specula were used; the infants' eyelids were held open with the imager's fingers during imaging. Artificial tears (sodium chloride solution, 0.9%) were usually applied to lubricate the cornea during imaging. Oral sucrose 24% with a pacifier was sometimes used to minimize infant stress.

We used a custom LabVIEW (LabVIEW 2016; National Instruments, Austin, TX, USA) program to acquire the OCTA images in this study. All OCTA volumes consisted of 400 B-scans with 400 A-scans per B-scan, and each B-scan was repeated four times at each location. The scanning time for each OCTA volume was 3.2 seconds.

OCTA Image Processing and Quantification

Custom MATLAB scripts (MATLAB 2018a; MathWorks, Natick, MA, USA) were employed to execute postprocessing of acquired OCTA volumes. A previously reported complex optical microangiography algorithm was utilized to extract blood flow information.[46,47] The retinal layer segmentation and motion corrections were implemented through a semiautomated segmentation program.[48] We did not segment by deep and superficial retinal capillary plexus since the vascular networks in individual retinal layers were underdeveloped, as previously described in newborns.[49,50] Instead, we reconstructed the angiogram with a nominal size of 7×7 mm^2, where the size was determined based on the axial eye length estimated from gestational age, including all retinal layers, in order to achieve adequate sampling for determination of retinal vascular parameters. The vasculature of all retinal layers was obtained as the maximum intensity projection of blood vessels between the internal limiting membrane and the outermost border of the outer nuclear layer, as shown in Figures 1A–C.

All OCTA images underwent a brief review to eliminate retinal angiograms with insufficient quality before proceeding to quantification of blood vessel parameters. The exclusion criteria included (1) no fovea captured in the OCTA volume, (2) disrupted main retinal vessels caused by large motion artifact, (3) distorted main retina vessels caused by infants visually following the scanning line during the OCTA volume acquisition, or (4) blur/fade microvasculature caused by inaccurate manual refractive error adjustments.

To ensure that the OCTA data acquired at various orientations were comparable between infants with various axial eye lengths, several calibrations on the retinal angiograms were implemented before vascular quantification, including (1) field-of-view calibration based on the axial length estimated from gestational age[51,52] and (2) anatomic position correction by leveling the central line between the optic disk and the fovea. The calibrated and reoriented retinal OCTA images were then put into a 10×10-mm blank frame (black background) and centered at the fovea for further quantification, as shown in Figure 1D. The foveal center was determined from the corresponding cross-sectional OCT structural volume as the location of the lowest point of the inner retina in cases of normal foveal contour or the highest point in cases of extensive cystoid macular edema.

To explore the retinal blood vessel differences between groups, four vascular morphology parameters were calculated: vessel area density,[53] nonperfusion area,[53] mean large vessel diameter,[53] and mean large vessel tortuosity.[54] Recognizing regional macular variability in vascular findings,[55,56] microvascular parameters (vessel area density and nonperfusion area) were evaluated based on the binarized vasculature map on the quadrant level. Quadrant-level analysis also allowed for the exclusion of quadrants with poor image quality. In order to explore differences in microvascular parameters based on location, we defined two nominal quadrant sizes: four small 1.5×1.5-mm^2 quadrants and four large 3×3-mm^2 quadrants (including the contents of the small quadrants) centered at the fovea (Fig. 1D). In contrast,

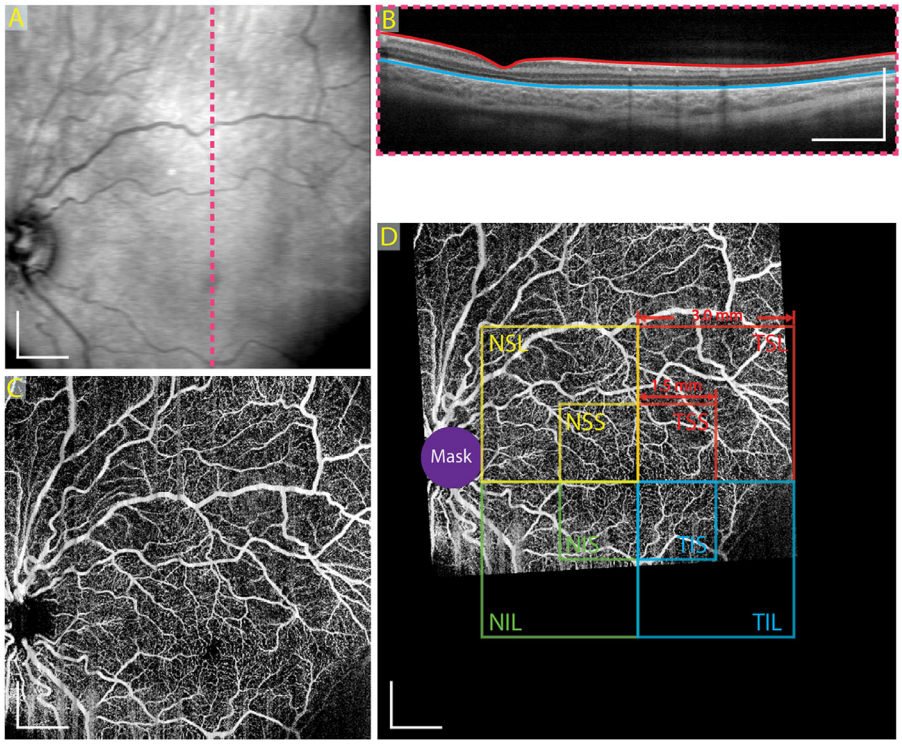

Figure 1. Neonatal swept-source optical coherence tomography angiography image processing. (A) En face projection of the retina, with a field of view of 7.05 × 7.05 mm, produced by mean intensity projection of the entire optical coherence tomography volume. (B) A selected cross-sectional B-scan (location indicated by the *red dashed line* in (A)) showing the center of the fovea with retinal segmentation overlay (*red solid line*, internal limiting membrane; *blue solid line*, outermost border of outer nuclear layer). (C) Corresponding retinal angiogram produced by maximum-intensity projection between the internal limiting membrane and outer nuclear layer. (D) Calibrated and reoriented retinal angiogram centered at the fovea in a 10 × 10-mm blank frame with both small and large quadrant segmentation shown. The retinal angiogram was reoriented by leveling the central line between the optic disk and the fovea. A disk-shaped mask with the same diameter as the optic disk was applied to exclude the vessels overlying the optic disk. All *scale bars* represent 1 mm. NIL, nasal inferior large; NIS, nasal inferior small; NSL, nasal superior large; NSS, nasal superior small; TIL, temporal inferior large; TIS, temporal inferior small; TSL, temporal superior large; TSS, temporal superior small.

the large-vessel parameters (mean large-vessel diameter and mean large-vessel tortuosity) were calculated based on the entire calibrated angiogram. Both retinal arteries and veins were included in the large-vessel parameter quantification. The mean large-vessel diameter was calculated using the same method as previously described.[53] However, we employed a vessel length filter of a minimum 200 µm. This threshold was subjectively selected by one of the authors (YC) to eliminate dense and short capillary vessels for optimal large-vessel visualization. Tortuosity was defined as the ratio of the length of the curve of a vessel segment over the distance between two ends of the curve.[54] The mean large-vessel tortuosity was calculated by averaging the local tortuosity values for each large-vessel branch. A disk-shaped mask with the same diameter as the optic disk was used to obscure the optic disk when quantifying the large-vessel parameters to eliminate analysis of vessels on the disk, as shown in Figure 1D.

Before proceeding to statistical analysis, all quantified OCTA images underwent an additional analysis to eliminate poor-quality quadrants. The exclusion criteria for quadrants were defined as more than 30% quadrant area missing blood vessel information (due to decentration or motion artifact caused by operator's hand or infant motion during acquisition) or low signal-to-noise ratio (SNR) of blood vessels in the quadrant (less than 80% of the average SNR of the entire OCTA image). The SNR of blood vessels was defined as $20 \times \log_{10} (I_{vessel}/I_{noise})$, where I_{vessel} represents the intensity of the blood vessels, and I_{noise} represents the intensity of the noise floor in the angiogram (i.e., intensity of the area without blood vessels).

Statistical Analysis

Excluding poor-quality quadrants, the intraobserver variation for each vascular quantification parameter was evaluated using the coefficient of

variation from two consecutive OCTA acquisitions in the same eye. After eliminating retinal angiograms with insufficient quality, microvascular parameters (i.e., vessel density and nonperfusion area) were compared between paired nasal and temporal quadrants (analysis separated by large and small quadrants, taking mean of any included superior and inferior quadrants) within premature and mature full-term infant groups, respectively, using a paired *t* test. Small- and large-vessel parameters quantified from high-quality retinal angiograms among all imaging sessions were compared between premature and mature full-term infants as well as between premature infants with and without advanced ROP (defined as stage 3 and/or pre-plus or worse ROP based on clinical indirect ophthalmoscopy). Due to the similarity between the superior and inferior macular regions, we grouped their microvascular quantification values together for these comparisons. The generalized linear mixed model was used to compare retinal blood vessel parameters between groups, accounting for nonindependence of multiple measurements (both eyes, quadrants, and visits) per infant. Statistical calculations for all blood vessel parameters were performed using SAS version 9.4 (SAS Institute, Inc., Cary, NC, USA), while the statistical analysis for the SNRs of the data set was performed on MATLAB 2018a (MathWorks) using the Wilcoxon rank-sum test. A two-sided *P* value of 0.05 was considered statistically significant.

Results

Study Participants

Demographic and clinical characteristics of all study participants are shown in Table 1. We obtained a total of 55 eye imaging volumes on eight preterm infants (mean gestational age 28 ± 4 weeks, birth weight 891 ± 314 g, and postmenstrual age at the first imaging session 37 ± 2 weeks) using the investigational handheld SS-OCTA. Each infant underwent a median of 1 (range, 1–4) imaging session on separate days, and a median of 3 (range, 2–9) volumes were obtained per imaging session. Three (20%) imaging sessions were rejected from a total of 15 imaging sessions due to insufficient quality. Among 45 eye volumes in the remaining 12 good imaging sessions, 14 (31%) were further rejected as they failed quantitative OCTA analysis. In the remaining 31 volumes, there were 11 (36%) right eyes, 7 (23%) stage 0, 8 (26%) stage 1, 13 (42%) stage 2, and 3 (9%) stage 3 ROP (based on indirect ophthalmoscopy). There were no cases of ROP or avascularity occurring in zone 1, but 16 (52%) occurred in zone 2 and 15 (48%) in zone 3. Only 3 (9%) eye images were obtained in the setting of pre–plus disease and none (0%) coincided with plus disease. Representative OCTA images for preterm infants are shown in Figures 2A–C.

We obtained a total of 54 eye imaging volumes of 12 full-term infants (mean gestational age 39 ± 1 weeks; birth weight 3405 ± 329 g) using the investigational handheld SS-OCTA. Each full-term infant underwent only one imaging session within the first 72 hours of life, with a median of 5 (range, 2–7) volumes obtained per imaging session. Of these, 6 (11%) volumes were rejected due to insufficient quality. In the remaining 48 volumes, 25 (52%) were performed on the right eye. Representative OCTA images for full-term infants are shown in Figures 2D–F.

Image Quality

For a total of 109 eye volumes from both preterm and full-term infants, 30 (28%) were rejected due to insufficient quality. Among these rejected volumes, 17 (57%) were rejected because the fovea was not captured, the primary reason for failure to perform retinal morphologic parameter analysis in this study. The second most common reason for insufficient quality was severe motion artifact in 9 (30%) volumes, which led to disrupted or distorted retinal vessels in the resultant OCTA angiograms. The third most common reason for failure of high-quality OCTA volume acquisition was inaccurate manual refractive error adjustments in 4 (13%) volumes, which resulted in blurred or faded microvascular networks in the projected angiogram.

For the remaining 79 high-quality OCTA volumes after field-of-view calibration and anatomic position correction, residual missing or low-image quality quadrants were eliminated from retinal vascular parameter analysis to further enhance image quality in the final analysis. Among 31 good-quality volumes from preterm infants, 20 of 62 (32%) temporal small quadrants, 11 of 62 (18%) nasal small quadrants, 42 of 62 (68%) temporal large quadrants, and 21 of 62 (34%) nasal large quadrants were excluded based on predetermined quadrant quality exclusion criteria (>30% quadrant area missing vessel information or <80% of average SNR for entire image). According to the same criteria, 15 of 96 (16%) temporal small quadrants, 33 of 96 (34%) nasal small quadrants, 47 of 96 (49%) temporal large quadrants, and 61 of 96 (64%) nasal large quadrants were excluded from 48 good-quality volumes obtained from full-term infants.

Among the remaining quadrants, the SNR calculation indicated that there was no significant difference

Table 1. Clinical Characteristics and Handheld Swept-Source Optical Coherence Tomography Angiography Findings of Preterm Infants Screened for ROP and Full-Term Normal Newborns

Characteristic	Preterm Infants ($n = 8$)		Full-Term Infants ($n = 12$)		
Demographic characteristic					
Male, No. (%) of infants	3 (38)		4 (33)		
Birth weight, mean (SD), g	891 (314)		3405 (329)		
Gestational age, mean (SD), wk	28 (4)		39 (1)		
Postmenstrual age at the first OCTA scan, mean (SD), wk	37 (2)		39 (1)		
Indirect ophthalmoscopic findings					
ROP stage, No. (%) of eye volumes	$n = 31$[a]				
Stage 0	7 (23)		NA		
Stage 1	8 (26)				
Stage 2	13 (42)				
Stage 3	3 (9)				
ROP zone, No. (%) of eye volumes					
Zone I	0 (0)		NA		
Zone II	16 (52)				
Zone III	15 (48)				
Pre–plus disease	3 (9)				
Plus disease	0 (0)				
Handheld SS-OCTA findings		*P* Value[b]		*P* Value[b]	*P* Value[c]
Vessel area density, mean (SD)[d]					
Temporal small quadrant	0.33 (0.10)	*0.850*	0.33 (0.09)	*0.915*	*0.886*
Nasal small quadrant	0.34 (0.11)		0.33 (0.12)		*0.773*
Temporal large quadrant	0.40 (0.08)	*0.558*	0.42 (0.11)	*0.096*	*0.403*
Nasal large quadrant	0.42 (0.12)		0.46 (0.09)		*0.129*
Nonperfusion area, mean (SD), mm^2[d]					
Temporal small quadrant	1.51 (0.22)	0.983	1.54 (0.21)	*0.849*	*0.509*
Nasal small quadrant	1.51 (0.27)		1.55 (0.26)		*0.490*
Temporal large quadrant	5.78 (0.69)	0.924	5.70 (0.91)	0.319	*0.740*
Nasal large quadrant	5.76 (0.83)		5.50 (0.95)		*0.208*
Large-vessel diameter, mean (SD), μm[e]	63.31 (6.21)	NA	67.32 (8.67)	NA	*0.081*
Large-vessel tortuosity, mean (SD), μm[e,f]	1.15 (0.04)	NA	1.12 (0.02)	NA	***0.004***

NA, not applicable; ROP, retinopathy of prematurity; SD, standard deviation; SS-OCTA, swept-source optical coherence tomography angiography; the bold and italic value in the table indicates the two-side *P* value less than 0.05.

[a]Total number of eye volumes among multiple eyes and visits per infant.

[b]Paired *t* test comparing nasal and temporal quadrants within each infant.

[c]Comparing preterm infants to full-term infants using a generalized linear mixed model accounting for nonindependence of multiple measurements (both eyes, quadrants, and visits) per infant.

[d]Calculated after excluding low-quality quadrants (>30% quadrant area missing vessel information or <80% of average signal-to-noise ratio for entire image) and grouping superior and inferior quadrants together (*n* ranges from 20 to 81).

[e]Calculated from entire en face image (preterm, $n = 31$; full-term, $n = 48$) as previously described.[53]

[f]Ratio of the length of the curve of a large vessel segment over the distance between two ends of the curve.[54]

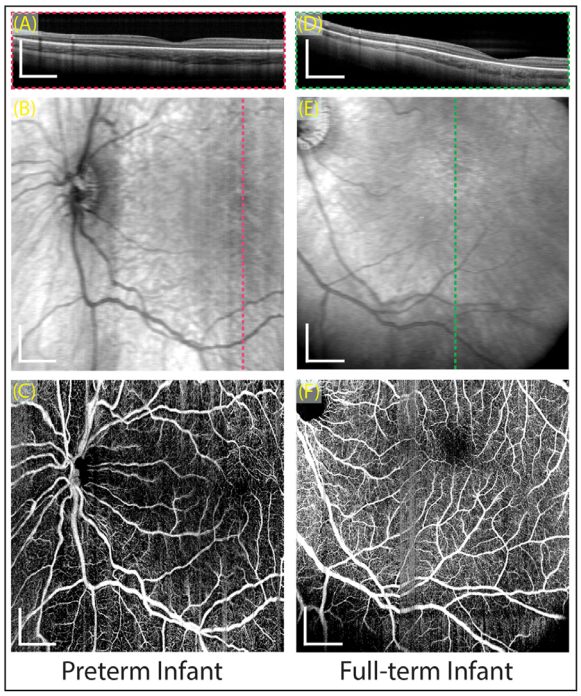

Figure 2. Representative swept-source optical coherence tomography angiography scans for nonsedated infants. (A, B) Selected cross-sectional B-scans passing through the foveal center in a preterm infant (A) born 28.3 weeks gestational age, 1164 g birth weight, with retinopathy of prematurity stage 0, zone 3, without pre–plus or plus disease and a full-term (B) newborn born, gestational age 37 weeks. The locations of these B-scans are indicated by the *dashed lines* in the en face projections (C, D). (C, D) En face projection of the retina for the preterm infant (C) with a field of view of 7.19 × 7.19 mm and for the full-term newborn (D) with a field of view of 6.91 × 6.91 mm. Both images were produced by mean intensity projection of the entire optical coherence tomography volume. (E, F) Corresponding retinal angiograms of the preterm infant (E) and full-term newborn (F) produced by maximum-intensity projection between the internal limiting membrane and outer nuclear layer. All *scale bars* represent 1 mm.

in the image quality between preterm (5.08 ± 1.52 dB) and full-term (4.90 ± 1.12 dB) infants (all $P > 0.05$, Table 2). Similarly, there was no significant difference in image quality between large quadrants of preterm infants with advanced ROP (7.19 dB for temporal large quadrants and 5.21 ± 0.74 dB for nasal large quadrants) and preterm infants without advanced ROP (5.25 ± 1.14 dB for temporal large quadrants and 5.16 ± 1.10 dB for nasal large quadrants, both $P > 0.05$, Table 2). The small quadrant image quality of preterm infants with advanced ROP was significantly greater than those without advanced ROP (temporal small quadrant, 11.80 ± 3.80 dB vs. 4.87 ± 1.35 dB, $P = 0.020$; nasal small quadrant, 6.46 ± 2.56 dB vs. 4.62 ± 1.22 dB, $P = 0.017$, respectively; Table 2). Nonetheless, no differences in microvascular parameters between the two groups were identified for the small quadrants (Table 4). Furthermore, the SNRs of all quadrants in both preterm subgroups were higher than 80% of the average SNR of the entire preterm data set (5.08 ± 1.52 dB, Table 2), and therefore, the quantification results were still regarded as valid.

Intraobserver Variation

Intraobserver variation (based on coefficient of variation) from repeated images taken during the same imaging session was calculated in a subset of five eyes (two right eyes, three left eyes) of three infants (two preterm infants, one full-term infant) for each vascular quantification parameter (Table 3). Among all eye quadrants, the intraobserver variation of vessel area density and nonperfusion area reached maximum values of 11.2% and 12.0%, respectively, which were felt to be acceptable. Large-vessel measurements were even more reliable. Among all five eyes, intraobserver variation of large-vessel diameter and tortuosity only reached maximum values of 3.9% and 1.8%, respectively.

OCTA Vascular Quantification

Values for all quantitative retinal vascular morphologic parameters are summarized in Table 1. Within each infant, comparing microvascular parameters between temporal and nasal quadrants (separately for large and small) revealed no significant differences for either preterm or full-term infants. The mean large-vessel tortuosity of the preterm infants (1.15 ± 0.04) was higher than that of full-term infants (1.12 ± 0.02, $P = 0.004$, Table 1). The large nasal quadrant vessel area density of preterm infants with advanced ROP (0.62 ± 0.26) was higher than those without advanced ROP (0.40 ± 0.10, $P = 0.007$, Table 4).

Other vascular quantification parameters, including mean large-vessel diameter, nonperfusion areas, and other quadrant vessel area densities, were not significantly different between preterm and full-term infants or between preterm infants with and without advanced ROP (Tables 1 and 4).

Discussion

This study presents handheld SS-OCTA for quantification of both large and small retinal blood vessel parameters in awake preterm and full-term newborn infants. Four OCTA quantitative parameters,

Table 2. Average Signal-to-Noise Ratio for Swept-Source Optical Coherence Tomography Angiography, Comparing Infant Groups

Characteristic	Preterm Infants ($n = 154$)		Full-Term Infants ($n = 228$)		*P* Value[a]
Average SNR, mean (SD), dB					
Temporal small quadrant	$n = 42$	5.16 (1.95)	$n = 81$	4.97 (1.02)	*0.835*
Nasal small quadrant	$n = 51$	4.84 (1.51)	$n = 63$	4.74 (1.28)	*0.696*
Temporal large quadrant	$n = 20$	5.35 (1.16)	$n = 49$	5.09 (1.01)	*0.570*
Nasal large quadrant	$n = 41$	5.16 (1.06)	$n = 35$	4.78 (1.08)	*0.123*
All quadrants	$n = 154$	5.08 (1.52)	$n = 228$	4.90 (1.12)	*0.427*
	Preterm Infants with Advanced ROP[b] ($n = 12$)		Preterm Infants without Advanced ROP[b] ($n = 142$)		*P* Value[a]
Average SNR, mean (SD), dB					
Temporal small quadrant	$n = 2$	11.11 (3.80)	$n = 40$	4.87 (1.35)	***0.020***
Nasal small quadrant	$n = 6$	6.46 (2.56)	$n = 45$	4.62 (1.22)	***0.017***
Temporal large quadrant	$n = 1$	7.19[c]	$n = 19$	5.25 (1.14)	*0.165*
Nasal large quadrant	$n = 3$	5.21 (0.74)	$n = 38$	5.16 (1.10)	*0.980*
All quadrants	$n = 12$	6.98 (2.92)	$n = 142$	4.92 (1.23)	***0.003***

n indicates the number of quadrants after eliminating quadrants of inadequate quality and merging results of superior and inferior quadrants from 8 preterm infants (1 preterm infant with advanced ROP and 7 without advanced ROP) and 12 full-term infants. dB, decibels; the bold and italic values in the table indicate two-side *P* values less than 0.05.

[a]*P* value obtained from the Wilcoxon rank-sum test using MATLAB 2018a.

[b]Advanced ROP defined as stage 3 and/or pre-plus or worse ROP.

[c]The standard deviation could not be calculated as only one value is in this quadrant.

Table 3. Intraobserver Error for Each Vascular Parameter Quantification in Subset of Five Eyes[a]

			Subject 1		Subject 2		Subject 3
Characteristic			Right Eye	Left Eye	Right Eye	Left Eye	Left Eye
Vessel area density	Temporal small quadrant	Scan 1	0.49	0.38	Excluded[b]	0.36	0.34
		Scan 2	0.49	0.46	Excluded[b]	0.38	0.43
		CoV	0.001	0.098	NA	0.022	0.112
	Nasal small quadrant	Scan 1	0.46	0.34	Excluded[b]	0.39	0.40
		Scan 2	0.41	0.38	Excluded[b]	0.44	0.45
		CoV	0.063	0.044	NA	0.060	0.055
	Temporal large quadrant	Scan 1	0.72	0.46	Excluded[b]	0.49	Excluded[b]
		Scan 2	0.83	0.45	Excluded[b]	0.49	Excluded[b]
		CoV	0.073	0.011	NA	0.002	NA
	Nasal large quadrant	Scan 1	0.45	Excluded[b]	Excluded[b]	0.42	0.49
		Scan 2	0.47	Excluded[b]	Excluded[b]	0.41	0.55
		CoV	0.019	NA	NA	0.008	0.060
Nonperfusion area (mm^2)	Temporal small quadrant	Scan 1	1.19	1.54	Excluded[b]	1.45	1.57
		Scan 2	1.30	1.35	Excluded[b]	1.48	1.31
		CoV	0.046	0.068	NA	0.010	0.090
	Nasal small quadrant	Scan 1	1.44	1.55	Excluded[b]	1.38	1.36
		Scan 2	1.47	1.42	Excluded[b]	1.24	1.22
		CoV	0.013	0.043	NA	0.056	0.056
	Temporal large quadrant	Scan 1	3.95	5.38	Excluded[b]	5.37	Excluded[b]
		Scan 2	3.10	5.36	Excluded[b]	5.73	Excluded[b]
		CoV	0.120	0.002	NA	0.032	NA
	Nasal large quadrant	Scan 1	5.78	Excluded[b]	Excluded[b]	5.38	5.02
		Scan 2	5.84	Excluded[b]	Excluded[b]	5.39	4.94
		CoV	0.006	NA	NA	0.000	0.009
Mean large-vessel diameter[c] (μm)		Scan 1	54.45	70.64	53.14	58.63	57.03
		Scan 2	58.81	67.44	53.01	58.98	59.22
		CoV	0.039	0.024	0.001	0.003	0.019
Mean large-vessel tortuosity[d]		Scan 1	1.09	1.10	1.14	1.16	1.12
		Scan 2	1.13	1.10	1.15	1.13	1.11
		CoV	0.018	0.003	0.003	0.013	0.002

[a]Subject 1 is full term; subjects 2 and 3 are preterm. CoV, coefficient of variation (low CoV represents high observer repeatability); NA, CoV value cannot be calculated due to lack of data after exclusion criteria were applied.

[b]More than 30% of quadrant area missing blood vessel information, or the signal-to-noise ratio of that quadrant was less than 80% of average signal-to-noise ratio for entire image.

[c]Calculated from large vessels as previously described.[53]

[d]Ratio of the length of the curve of a large-vessel segment over the distance between two ends of the curve.[54]

including vessel area density, nonperfusion area, mean large-vessel diameter, and mean large-vessel tortuosity, were evaluated among 79 OCTA volumes.

Outside of measuring the FAZ, no prior studies performed quantification of retinal morphologic parameters (microvasculature or large vessel) from OCTA images in the preterm infant population. A recent study from Falavarjani et al.[57] evaluated the OCTA of children ages 4 to 12 years and demonstrated a higher mean central foveal vessel area density in ex-preterm infants compared with that of ex-full-term infants ($P < 0.001$), negatively correlating these parameters to gestational age ($P = 0.001$) and birth weight ($P = 0.002$). We observed a similar pattern for the nasal large quadrant vessel area density between preterm infants with advanced ROP and preterm infants without advanced ROP in the present study ($P = 0.007$, Table 4). When comparing preterm infants screened for ROP to full-term normal newborns, we identified increased tortuosity in the preterm group ($P = 0.004$, Table 1), although absolute differences were small. While not powered to identify associations with plus or pre–plus disease, these findings suggest that OCTA has the potential to identify important markers of ROP severity among awake preterm infants. Currently, the gold standard for ROP screening is fundus examination with binocular indirect ophthalmoscopy (BIO)[58] and, more recently, wide-field retinal photography.[59,60] Both BIO and wide-field retinal photography are uncomfortable procedures involving an eyelid speculum and ocular contact, with high interobserver disagreement.[61–65] Along with several

Table 4. Comparison of Handheld Optical Coherence Tomography Angiography Vascular Quantification Results Between Preterm Infants with and without Advanced Retinopathy of Prematurity[a]

Handheld SS-OCTA Findings	Preterm Infants with Advanced ROP ($n = 12$)		Preterm Infants without Advanced ROP ($n = 142$)		*P* Value
Vessel area density, mean (SD)					
Temporal small quadrant	$n = 2$	0.25 (0.07)	$n = 40$	0.34 (0.10)	*0.203*
Nasal small quadrant	$n = 6$	0.28 (0.10)	$n = 45$	0.34 (0.11)	*0.402*
Temporal large quadrant	$n = 1$	0.34 (NA)	$n = 19$	0.40 (0.08)	*NA*
Nasal large quadrant	$n = 3$	0.62 (0.26)	$n = 38$	0.40 (0.10)	***0.007***
Nonperfusion area, mean (SD), mm^2					
Temporal small quadrant	$n = 2$	1.71 (0.24)	$n = 40$	1.50 (0.22)	*0.274*
Nasal small quadrant	$n = 6$	1.71 (0.23)	$n = 45$	1.48 (0.27)	*0.279*
Temporal large quadrant	$n = 1$	5.85 (NA)	$n = 19$	5.78 (0.71)	*NA*
Nasal large quadrant	$n = 3$	5.00 (1.17)	$n = 38$	5.82 (0.79)	*0.083*
Large-vessel diameter,[b] mean (SD), µm	$n = 3$	63.22 (11.0)	$n = 28$	63.32 (5.82)	*0.893*
Large-vessel tortuosity,[c] mean (SD)	$n = 3$	1.15 (0.03)	$n = 28$	1.15 (0.05)	*0.944*

n indicates the number of quadrants after eliminating quadrants of inadequate quality and merging results of superior and inferior quadrants from 1 infant with advanced ROP and 7 infants without advanced ROP. NA, not applicable since *P* value cannot be calculated due to limited data; the bold and italic value in the table indicates the two-side *P* value less than 0.05.

[a]Advanced ROP defined as stage 3 and/or pre-plus or worse ROP.

[b]Calculated from large vessels of entire en face image as previously described.[53]

[c]Ratio of the length of the curve of a large-vessel segment over the distance between two ends of the curve.[54]

OCT structural findings associated with ROP severity that have already been identified,[8,12] OCTA objective quantitative parameters should be explored to identify additional potential ROP severity biomarkers. Noncontact handheld SS-OCTA may therefore serve as a potential ROP screening tool.

There are several limitations in this study. First, the success rate for acquiring high-quality OCTA volumes in nonsedated infants was low, primarily due to decentration, which highlights the inherent challenges involved in capturing the region of interest in an uncooperative awake infant. Motion artifacts also reduced the image quality in acquired OCTA volumes. Although an acquisition time of 3.8 seconds per volume is acceptable in the adult population,[22] it may not be sufficient for nonsedated infants. Further reducing the acquisition time by optimizing the scanning protocol or using a swept-source laser with a higher scanning rate may help mitigate this problem. In terms of refractive error adjustments, an autofocus module may help to improve the accuracy.

By excluding images with low quality at the quadrant level, we believe that this study minimizes bias since we do not expect a systematic disruption of image quality in particular regions of the retina relative to others. Following these exclusions, this device achieved adequate SNR and repeatability in awake infants for quantitative retinal vascular parameter analysis.

A small sample size along with difficulty in imaging younger preterm infants and those with severe ROP, which may be caused by smaller palpebral fissures, media opacity, and clinical instability, limited the statistical power to identify associations between retinal vascular parameters and plus or pre–plus disease in this study. As a pilot exploratory study, this work serves as a starting point for quantitative OCTA imaging among nonsedated infants. Future larger studies may further correlate these OCT parameters with ROP severity in a broader preterm population.

In conclusion, we are unaware of previous reports describing quantitative analysis of the vasculature in preterm infants using handheld SS-OCTA (PubMed search terms: optical coherence tomography angiography AND pediatric). Large- and small-vessel parameters have the potential to indicate ROP severity, pending further improvements to handheld OCTA technology.

Acknowledgments

Supported by the Knights Templar Eye Foundation; the Latham Foundation; Washington Research Foundation, Seattle, Washington; unrestricted grants from Research to Prevent Blindness; and the NIH CORE grant (EY001730) to the UW Department of Ophthalmology.

Disclosure: **K. Zhou,** None; **S. Song,** None; **A. Legocki,** None; **Y. Cheng,** None; **L. Ding,** None; **K.A. Rezaei,** None; **R.K. Wang,** the Oregon Health and Science University (P), the University of Washington (P), Carl Zeiss Meditec Inc (C, F), Colgate Palmolive Company (F), Moptim Inc (F), Facebook technologies LLC (F), Insight Photonic Solutions (C); **M.T. Cabrera,** None

References

1. Hartnett ME, Penn JS. Mechanisms and management of retinopathy of prematurity. *N Engl J Med*. 2012;367(26):2515–2526.
2. Valikodath N, Cole E, Chiang M, Campbell J, Chan R. Imaging in retinopathy of prematurity. *Asia Pac J Ophthalmol*. 2019;8(2):178–186.
3. Kim SJ, Port AD, Swan R, Campbell JP, Chan RP, Chiang MF. Retinopathy of prematurity: a review of risk factors and their clinical significance. *Surv Ophthalmol*. 2018;63(5):618–637.
4. Early Treatment for Retinopathy of Prematurity Cooperative Group. The incidence and course of retinopathy of prematurity: findings from the early treatment for retinopathy of prematurity study. *Pediatrics*. 2005;116(1):15–23.
5. Gilbert C, Fielder A, Gordillo L, et al. Characteristics of infants with severe retinopathy of prematurity in countries with low, moderate, and high levels of development: implications for screening programs. *Pediatrics*. 2005;115(5):e518–e525.
6. Maldonado RS, Toth CA. Optical coherence tomography in retinopathy of prematurity: looking beyond the vessels. *Clin Perinatol*. 2013;40(2):271–296.
7. Mallipatna A, Vinekar A, Jayadev C, et al. The use of handheld spectral domain optical coherence tomography in pediatric ophthalmology practice: our experience of 975 infants and children. *Indian J Ophthalmol*. 2015;63(7):586.
8. Legocki AT, Zepeda EM, Gillette TB, et al. Vitreous findings by handheld spectral domain optical coherence tomography correlate with retinopathy of prematurity severity. *Ophthalmol Retina*. 2020;4(10):1008–1015.
9. Muni RH, Kohly RP, Charonis AC, Lee TC. Retinoschisis detected with handheld spectral-domain optical coherence tomography in neonates with advanced retinopathy of prematurity. *Arch Ophthalmol*. 2010;128(1):57–62.
10. Chavala SH, Farsiu S, Maldonado R, Wallace DK, Freedman SF, Toth CA. Insights into advanced retinopathy of prematurity using handheld spectral domain optical coherence tomography imaging. *Ophthalmology*. 2009;116(12):2448–2456.
11. Lee AC, Maldonado RS, Sarin N, et al. Macular features from spectral domain optical coherence tomography as an adjunct to indirect ophthalmoscopy in retinopathy of prematurity. *Retina (Philadelphia, Pa.)*. 2011;31(8):1470.
12. Maldonado RS, Yuan E, Tran-Viet D, et al. Three-dimensional assessment of vascular and perivascular characteristics in subjects with retinopathy of prematurity. *Ophthalmology*. 2014;121(6):1289–1296.
13. Zepeda EM, Shariff A, Gillette TB, et al. Vitreous bands identified by handheld spectral-domain optical coherence tomography among premature infants. *JAMA Ophthalmol*. 2018;136(7):753–758.
14. Ells AL, Holmes JM, Astle WF, et al. Telemedicine approach to screening for severe retinopathy of prematurity: a pilot study. *Ophthalmology*. 2003;110(11):2113–2117.
15. Wu C, Petersen RA, VanderVeen DK. RetCam imaging for retinopathy of prematurity screening. *J Am Assoc Pediatr Ophthalmol Strabismus*. 2006;10(2):107–111.
16. Ng EY, Lanigan B. Fundus fluorescein angiography in the screening for and management of retinopathy of prematurity. *J Pediatr Ophthalmol Strabismus*. 2006;43(2):85–90.
17. Yokoi T, Hiraoka M, Miyamoto M, et al. Vascular abnormalities in aggressive posterior retinopathy of prematurity detected by fluorescein angiography. *Ophthalmology*. 2009;116(7):1377–1382.
18. Campbell JP, Nudleman E, Yang J, et al. Handheld optical coherence tomography angiography and ultra–wide-field optical coherence tomography in retinopathy of prematurity. *JAMA Ophthalmol*. 2017;135(9):977–981.
19. Yang J, Liu L, Campbell JP, Huang D, Liu G. Handheld optical coherence tomography angiography. *Biomed Optics Express*. 2017;8(4):2287–2300.
20. Viehland C, LaRocca F, Tran-Viet D, et al. Imaging of pediatric pathology in the intensive care

nursery using a custom handheld, ultra-compact, swept-source OCT probe (conference presentation). In: Manns F, Söderberg PG, Ho A eds. *Ophthalmic Technologies XXVIII*. San Francisco, CA, USA: International Society for Optics and Photonics; 2018.
21. Viehland C, Chen X, Tran-Viet D, et al. Ergonomic handheld OCT angiography probe optimized for pediatric and supine imaging. *Biomed Optics Express*. 2019;10(5):2623–2638.
22. Song S, Zhou K, Xu JJ, Zhang Q, Lyu S, Wang R. Development of a clinical prototype of a miniature hand-held optical coherence tomography probe for prematurity and pediatric ophthalmic imaging. *Biomed Optics Express*. 2019;10(5):2383–2398.
23. Hsu ST, Chen X, Ngo HT, et al. Imaging infant retinal vasculature with OCT angiography. *Ophthalmol Retina*. 2019;3(1):95.
24. Hsu ST, Ngo HT, Stinnett SS, et al. Assessment of macular microvasculature in healthy eyes of infants and children using OCT angiography. *Ophthalmology*. 2019;126(12):1703–1711.
25. Vinekar A, Chidambara L, Jayadev C, et al. Monitoring neovascularization in aggressive posterior retinopathy of prematurity using optical coherence tomography angiography. *J Am Assoc Pediatr Ophthalmol Strabismus*. 2016;20(3):271–274.
26. Kothari N, Chu A, Huang JM, et al. Arm-mounted optical coherence tomography angiography in extremely low birth weight neonates with retinopathy of prematurity. *Am J Ophthalmol Case Rep*. 2020;18:100624.
27. Moshiri Y, Legocki AT, Zhou K, et al. Handheld swept-source optical coherence tomography with angiography in awake premature neonates. *Quant Imaging Med Surg*. 2019;9(9):1495.
28. Kashani AH, Chen C-L, Gahm JK, et al. Optical coherence tomography angiography: a comprehensive review of current methods and clinical applications. *Prog Retin Eye Res*. 2017;60:66–100.
29. Binotti WW, Romano AC. Projection-resolved optical coherence tomography angiography parameters to determine severity in diabetic retinopathy. *Invest Ophthalmol Vis Sci*. 2019;60(5):1321–1327.
30. Kim AY, Chu Z, Shahidzadeh A, Wang RK, Puliafito CA, Kashani AH. Quantifying microvascular density and morphology in diabetic retinopathy using spectral-domain optical coherence tomography angiography. *Invest Ophthalmol Vis Sci*. 2016;57(9):OCT362–OCT370.
31. Lin AD, Lee AY, Zhang Q, et al. Association between OCT-based microangiography perfusion indices and diabetic retinopathy severity. *Br J Ophthalmol*. 2017;101(7):960–964.
32. Shao Q, Heussen FM, Ouyang Y, Hager A. Retinal vessel diameter changes in different severities of diabetic retinopathy by SD-OCT. *Eur J Ophthalmol*. 2016;26(4):342–346.
33. Bojikian KD, Chen C-L, Wen JC, et al. Optic disc perfusion in primary open angle and normal tension glaucoma eyes using optical coherence tomography-based microangiography. *PLoS One*. 2016;11(5):e0154691.
34. Yarmohammadi A, Zangwill LM, Diniz-Filho A, et al. Optical coherence tomography angiography vessel density in healthy, glaucoma suspect, and glaucoma eyes. *Invest Ophthalmol Vis Sci*. 2016;57(9):OCT451–OCT459.
35. Akil H, Huang AS, Francis BA, Sadda SR, Chopra V. Retinal vessel density from optical coherence tomography angiography to differentiate early glaucoma, pre-perimetric glaucoma and normal eyes. *PLoS One*. 2017;12(2):e0170476.
36. Chen C-L, Bojikian KD, Gupta D, et al. Optic nerve head perfusion in normal eyes and eyes with glaucoma using optical coherence tomography-based microangiography. *Quant Imaging Med Surg*. 2016;6(2):125.
37. Chen C-L, Zhang A, Bojikian KD, et al. Peripapillary retinal nerve fiber layer vascular microcirculation in glaucoma using optical coherence tomography–based microangiography. *Invest Ophthalmol Vis Sci*. 2016;57(9):OCT475–OCT485.
38. Bojikian KD, Nobrega P, Wen JC, et al. Macular Vascular microcirculation in eyes with open-angle glaucoma using different visual field severity classification systems. *J Glaucoma*. 2019;28(9):790–796.
39. Richter GM, Sylvester B, Chu Z, et al. Peripapillary microvasculature in the retinal nerve fiber layer in glaucoma by optical coherence tomography angiography: focal structural and functional correlations and diagnostic performance. *Clin Ophthalmol (Auckland, NZ)*. 2018;12:2285.
40. Chang M, Yoo C, Kim S-W, Kim YY. Retinal vessel diameter, retinal nerve fiber layer thickness, and intraocular pressure in Korean patients with normal-tension glaucoma. *Am J Ophthalmol*. 2011;151(1):100–105.e1.
41. Sasongko M, Wong T, Nguyen T, Cheung C, Shaw J, Wang J. Retinal vascular tortuosity in persons with diabetes and diabetic retinopathy. *Diabetologia*. 2011;54(9):2409–2416.
42. Lee H, Lee M, Chung H, Kim HC. Quantification of retinal vessel tortuosity in diabetic retinopathy using optical coherence tomography angiography. *Retina*. 2018;38(5):976–985.

43. Saraf SS, Tyring AJ, Chen C-L, et al. Familial retinal arteriolar tortuosity and quantification of vascular tortuosity using swept-source optical coherence tomography angiography. *Am J Ophthalmol Case Rep*. 2019;14:74–78.
44. Shahlaee A, Hong BK, Ho AC. Optical coherence tomography angiography features of branch retinal vein occlusion. *Retin Cases Brief Rep*. 2017;11(1):90–93.
45. White I, Dederich H. *American National Standard for Safe Use of Lasers, ANSI Z 136.1–2007*. Orlando, FL: Laser Institute of America; 2007.
46. Wang RK, An L, Francis P, Wilson DJ. Depth-resolved imaging of capillary networks in retina and choroid using ultrahigh sensitive optical microangiography. *Opt Lett*. 2010;35(9):1467–1469.
47. Zhang Q, Wang J, Wang RK. Highly efficient eigen decomposition based statistical optical microangiography. *Quant Imaging Med Surg*. 2016;6(5):557.
48. Yin X, Chao JR, Wang RK. User-guided segmentation for volumetric retinal optical coherence tomography images. *J Biomed Optics*. 2014;19(8):086020.
49. Fruttiger M. Development of the retinal vasculature. *Angiogenesis*. 2007;10(2):77–88.
50. Gariano RF, Iruela-Arispe ML, Hendrickson AE. Vascular development in primate retina: comparison of laminar plexus formation in monkey and human. *Invest Ophthalmol Vis Sci*. 1994;35(9):3442–3455.
51. Maldonado RS, Izatt JA, Sarin N, et al. Optimizing hand-held spectral domain optical coherence tomography imaging for neonates, infants, and children. *Invest Ophthalmol Vis Sci*. 2010;51(5):2678–2685.
52. Cook A, White S, Batterbury M, Clark D. Ocular growth and refractive error development in premature infants with or without retinopathy of prematurity. *Invest Ophthalmol Vis Sci*. 2008;49(12):5199–207.
53. Chu Z, Lin J, Gao C, et al. Quantitative assessment of the retinal microvasculature using optical coherence tomography angiography. *J Biomed Opt*. 2016;21(6):66008.
54. Hart WE, Goldbaum M, Cote B, Kube P, Nelson MR. Measurement and classification of retinal vascular tortuosity. *Int J Med Inform*. 1999;53(2–3):239–52.
55. Hou H, Moghimi S, Zangwill LM, et al. Macula vessel density and thickness in early primary open-angle glaucoma. *Am J Ophthalmol*. 2019;199:120–132.
56. Shin JW, Lee J, Kwon J, Choi J, Kook MS. Regional vascular density–visual field sensitivity relationship in glaucoma according to disease severity. *Br J Ophthalmol*. 2017;101(12):1666–1672.
57. Falavarjani KG, Iafe NA, Velez FG, et al. Optical coherence tomography angiography of the fovea in children born preterm. *Retina*. 2017;37(12):2289–2294.
58. Fierson WM; American Academy of Pediatrics Section on Ophthalmology; American Academy of Ophthalmology; American Association for Pediatric Ophthalmology and Strabismus; American Association of Certified Orthoptists. Screening examination of premature infants for retinopathy of prematurity. *Pediatrics*. 2018;142(6):e20183061.
59. Quinn GE, Ying GS, Daniel E, Hildebrand PL, Ells A, Baumritter A, Kemper AR, Schron EB, Wade K, e ROP Cooperative Group. Validity of a telemedicine system for the evaluation of acute-phase retinopathy of prematurity. *JAMA Ophthalmol*. 2014;132(10):1178–1184.
60. Fierson WM; American Academy of Pediatrics Section on Ophthalmology; American Academy of Ophthalmology; American Association for Pediatric Ophthalmology and Strabismus; American Association of Certified Orthoptists. Screening examination of premature infants for retinopathy of prematurity. *Pediatrics*. 2013;131(1):189–195.
61. Chiang MF, Jiang L, Gelman R, Du YE, Flynn JT. Interexpert agreement of plus disease diagnosis in retinopathy of prematurity. *Arch Ophthalmol*. 2007;125(7):875–80.
62. Wallace DK, Quinn GE, Freedman SF, Chiang MF. Agreement among pediatric ophthalmologists in diagnosing plus and pre-plus disease in retinopathy of prematurity. *J Am Assoc Pediatr Ophthalmol Strabismus*. 2008;12(4):352–356.
63. Hewing NJ, Kaufman DR, Chan RP, Chiang MF. Plus disease in retinopathy of prematurity: qualitative analysis of diagnostic process by experts. *JAMA Ophthalmol*. 2013;131(8):1026–1032.
64. Scott KE, Kim DY, Wang L, et al. Telemedical diagnosis of retinopathy of prematurity: intraphysician agreement between ophthalmoscopic examination and image-based interpretation. *Ophthalmology*. 2008;115(7):1222–1228.e3.
65. Gschließer A, Stifter E, Neumayer T, et al. Inter-expert and intra-expert agreement on the diagnosis and treatment of retinopathy of prematurity. *Am J Ophthalmol*. 2015;160(3):553–560.e3.